Volume 17 | Number 15 | 7 August 2017 | Pages 2531–2684

Lab on a Chip

Devices and applications at the micro- and nanoscale

rsc.li/loc

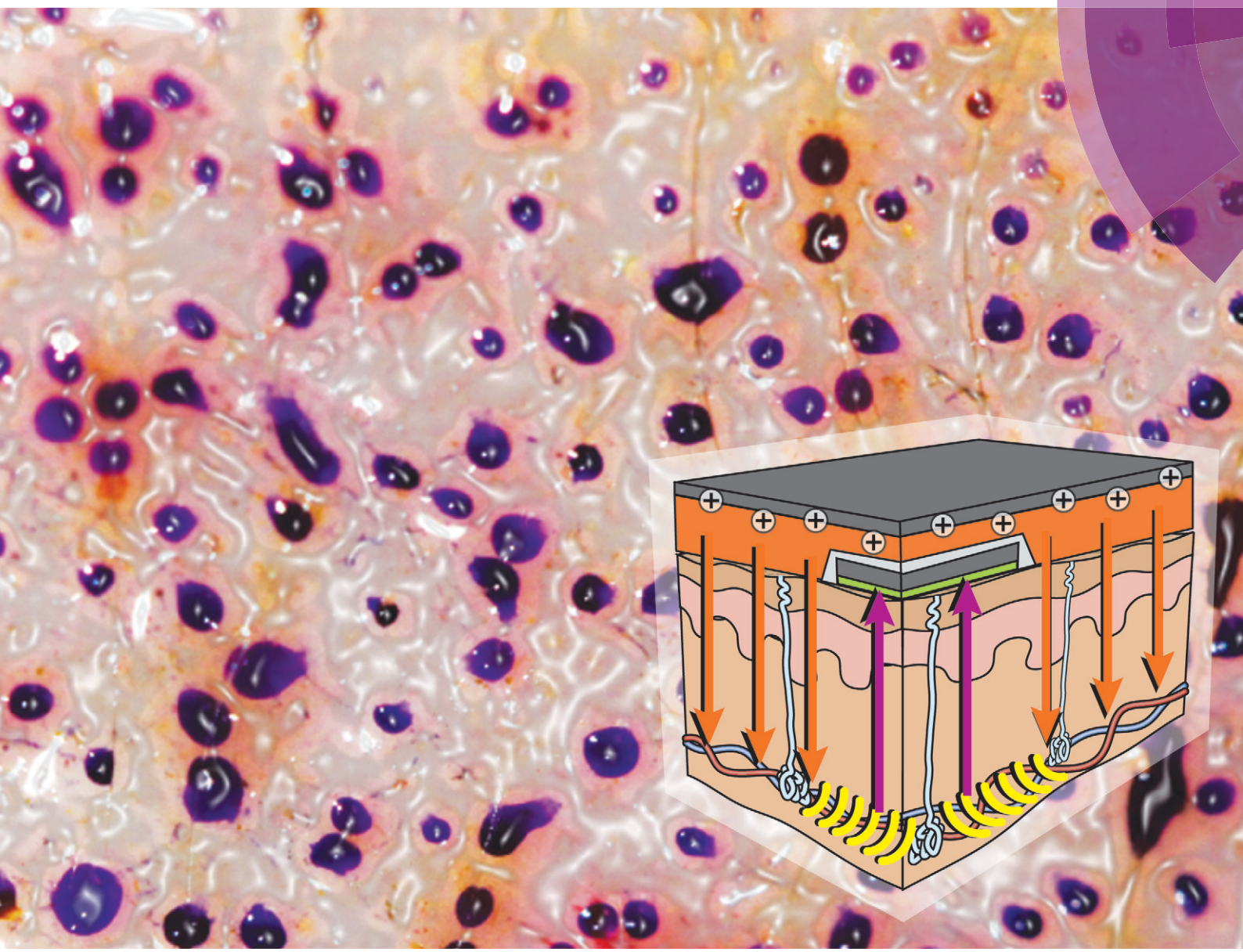

ISSN 1473-0197

ROYAL SOCIETY OF CHEMISTRY

PAPER

Jason Heikenfeld *et al.*

Integrated sudomotor axon reflex sweat stimulation for continuous sweat analyte analysis with individuals at rest

Lab on a Chip

PAPER

View Article Online
View Journal | View Issue

Check for updates

Cite this: *Lab Chip*, 2017, **17**, 2550

Integrated sudomotor axon reflex sweat stimulation for continuous sweat analyte analysis with individuals at rest†

Zachary Sonner,[a] Eliza Wilder,[b] Trudy Gaillard,[c] Gerald Kasting[b] and Jason Heikenfeld*[a]

Received 3rd April 2017,
Accepted 26th June 2017

DOI: 10.1039/c7lc00364a

rsc.li/loc

Eccrine sweat has rapidly emerged as a non-invasive, ergonomic, and rich source of chemical analytes with numerous technological demonstrations now showing the ability for continuous electrochemical sensing. However, beyond active perspirers (athletes, workers, *etc.*), continuous sweat access in individuals at rest has hindered the advancement of both sweat sensing science and technology. Reported here is integration of sudomotor axon reflex sweat stimulation for continuous wearable sweat analyte analysis, including the ability for side-by-side integration of chemical stimulants & sensors without cross-contamination. This integration approach is uniquely compatible with sensors which consume the analyte (enzymatic) or sensors which equilibrate with analyte concentrations. *In vivo* validation is performed using iontophoretic delivery of carbachol with ion-selective and impedance sensors for sweat analysis. Carbachol has shown prolonged sweat stimulation in directly stimulated regions for five hours or longer. This work represents a significant leap forward in sweat sensing technology and may be of broader interest to those interested in on-skin sensing integrated with drug delivery.

Published on 04 July 2017. Downloaded by UNIVERSITY OF CINCINNATI on 25/07/2017 20:27:51.

Reprinted From Lab on a Chip

Introduction

Biosensing for medical and wearables applications has shown surging interest in recent years.[2–4] Blood analysis remain the gold-standard for systemic biomarker concentrations. However, blood sampling is invasive and therefore difficult and/or undesirable to implement for continuous sensing of analytes. Recently, eccrine sweat has emerged as an analyte-rich alternative[5–10] to blood and other biofluids; with numerous wearable sweat analysis devices previously demonstrated.[11–17] Yet, few of these wearable devices initiate sweating, rather they require the user to perform exercises or otherwise increase body temperature to cause sweat generation across most of the body. However, chemical sweat stimulation is used commercially in a point-of-care test for cystic fibrosis *via* estimation of Cl^- concentrations in sweat by electrical conductivity analysis. In this cystic fibrosis test, iontophoresis[18,19] is used to deliver positively-charged pilocarpine (Table 1, $pK_a \approx 7$)[20] into the skin which causes localized sweat generation[21] (ηL's min^{-1} per gland). This test is not analyte-specific and is cumbersome: a wired iontophoresis device with pilocarpine-containing hydrogel is strapped to the skin, iontophoresis is performed, the gels removed, a wired sweat conductivity analyzer is applied over the stimulation site, and after several minutes conductivity measurements are performed. It is likely that most of the applications for sensing sweat analytes will be outside of one-time samplings (which blood or other biofluids[5,22] can easily provide) and will be beyond active perspirers such as athletes or workers, therefore, requiring sweat stimulation.[5,22]

Just recently, a fully integrated device was reported that can automatically stimulate and measure changes in sweat ethanol with good correlation to changes in blood or breath concentration.[23] However, this approach has at least two potentially significant unresolved challenges. First, the sweat

Table 1 Potential cholinomimetic stimulants[1]

Stimulant	Specificity		
	Nicotinic	Muscarinic	AChE hydrolysis
Acetylcholine	+++	+++	+++
Carbachol	+++	++	–
Methacholine	+	+++	++
Pilocarpine	–	++	–

Here, increasing '+' indicates stronger interaction and '–' is weak interaction.

[a] *Department of Electrical Engineering & Computer Systems, University of Cincinnati, Cincinnati, OH, 45221, USA. E-mail: heikenjc@ucmail.uc.edu; Tel: +513 556 4763*
[b] *Winkle College of Pharmacy, University of Cincinnati, Cincinnati, OH, 45267, USA*
[c] *College of Nursing, University of Cincinnati, Cincinnati, Ohio, 45221, USA*
† Electronic supplementary information (ESI) available. See DOI: 10.1039/c7lc00364a

This journal is © The Royal Society of Chemistry 2017

Published on 04 July 2017. Downloaded by UNIVERSITY OF CINCINNATI on 25/07/2017 20:27:51.

stimulant was pilocarpine which rapidly raises the sweat generation rate but leads to gradual decay over 30–90 minutes to an unusable or miniscule sweat generation rate. Although repeated sweat stimulation to allow prolonged monitoring is possible, less iontophoresis is always preferred (less possible irritation, pain, and/or damage to the skin). Second, and even more challenging, the enzymatic ethanol sensor was co-located within a hydrogel reservoir of pilocarpine. Although this allows integration of stimulation and sensing onto the same skin site, it also causes an unpredictable amount of analyte dilution. For example, if sweat generation rate increases/decreases, more/less analyte is brought to the enzymatic sensor (be it for glucose, ethanol, lactate, *etc.*) and the enzymatic sensor which continually consumes the analyte[3,24] will give a false higher/lower reading. Historically interesting, for this very reason, sweat was a leading confounding factor for the failed non-invasive GlucoWatch Biographer which extracted glucose by reverse iontophoresis.[25] Problems could be potentially worse for non-enzymatic sensors (ion-selective,[24] aptamer,[24] *etc.*) because such sensors don't consume the analyte, they instead need to equilibrate to the concentration of the analyte in the sample. For example, if a hydrogel were only 1 mm thick and at 0.1 to 1 $\eta L\ min^{-1}$ per gland and 100 glands per cm^2, it could require somewhere from 1000 to 10 000 minutes for analyte concentrations in the hydrogel to fully equilibrate towards their actual concentrations in sweat (assumes 100% of hydrogel volume filled/exchanged).

Another recent demonstration utilized separated sensing and stimulation regions, with acetylcholine, pilocarpine, or methacholine as the primary agonists.[26] *In vivo* Na^+ and Cl^- data was collected using methacholine, which at best will induce a weaker SAR response (Table 1). In this work, they suggest that the main mechanism of stimulation is using iontophoresis to drive the stimulant horizontally over long distance through skin beneath the sensors. Such horizontal iontophoresis is an assumption that is in conflict with conventional understanding of iontophoresis into the skin.[27] Rather, because their integration leveraged a thin-film wick (rayon), it is possible that sweat generation was primarily under the stimulation electrode and simply wicked horizontally from the point of sweat generation to the sensors. Furthermore, the device utilized no fluidic isolation mechanism (*i.e.*, adhesive) to directly separate the stimulation and sensing regions, bringing rise to the same challenges discussed in the previous paragraph. Clearly, integration of sweat stimulation and sensing remains a significant unresolved challenge.

Presented here is a system leveraging both a unique device architecture and novel sweat stimulation technique which overcomes several, previous limitations towards continuous and convenient sweat stimulation and sensing for resting individuals. The sweat stimulation technique exploits an underutilized pharmacological phenomenon called sudomotor axon reflex (SAR) sweating. While typically used for assessing autonomic nervous system disorders, this method produces a unique sweating response with sweat produced directly underneath the stimulation area and sweat produced in the periphery.[27,28] This response is produced *via* iontophoresis of a nicotinic agonist through the skin.[27] Utilizing the device developed here as an example, shown in Fig. 1a, a gel is placed over the wearable device with iontophoretic current passing through openings in the substrate adjacent to sensor(s). As shown in Fig. 1b, the nicotinic agonist interacts with the nicotinic receptor(s) presumably at the base of the gland where the majority of nerve fibers are located,[29,30] causing axonal conduction towards branch points. Here, a portion of secondary signals are redirected orthodromically towards sweat glands in the periphery, thereby eliciting an indirect response (axon reflex).[28,31] Stimulants that target nicotinic receptors have been shown to produce a strong SAR response,[27,32] compared to those which act primarily on muscarinic receptors (see Table 1 for common muscarinic/nicotinic agonists, adapted from Rang[1]). Detailed mechanisms including pharmacology for SAR sweating have been previously described in literature.[27,28,31–33] Thus, this technique allows sweat to be produced underneath sensors without direct interference from the stimulation region. In other words, this allows the direct stimulation region and sensing areas to remain separated, which should reduce sensor contamination and/or dilution from the stimulant-containing gel and promote the development of a single step, integrated device.

Reprinted From Lab on a Chip

Experimental

Reagents and materials

Carbachol 99% (CAS 51-83-2) was purchased from Professional Compounding Centers of America (PCCA, Houston, TX). Agarose (A9539) and bromophenol blue (B0126) was purchased from Sigma Aldrich (St. Louis, MO). 5000 cSt and 100 cSt cosmetic-grade polydimethylsiloxane (PDMS) was purchased from ClearCo Products (Willow Grove, PA). Polyethylene terephthalate (PET, 3 mil) was purchased from McMaster Carr (Aurora, OH). Screen-printable silver/silver-chloride (CI-4001) and carbon (CI-2001) inks were purchased from Engineered Conductive Materials (Delaware, OH). Screen printable solder mask (FOC-800) was purchased from Taiyo America (Carson City, NV). *Z*-Axis conductive tape (9703) and double sided medical adhesive (1577) was provided by 3M Medical Specialties (St. Paul, MN).

Instrumentation

Sodium sensor and Ag/AgCl reference potential measurements, including calibration, occurred using a precision data acquisition system (EMF6, Lawson Labs Inc., Malvern, PA). Monitoring of the impedance sensors was performed using a multipurpose electrochemical unit (Palmsens3, PalmSens BV, Houten, Netherlands). Iontophoresis was performed utilizing an iontophoretic unit with current and dosage controls (ActivaDose II, ActivaTek, Gilroy, CA).

Published on 04 July 2017. Downloaded by UNIVERSITY OF CINCINNATI on 25/07/2017 20:27:51.

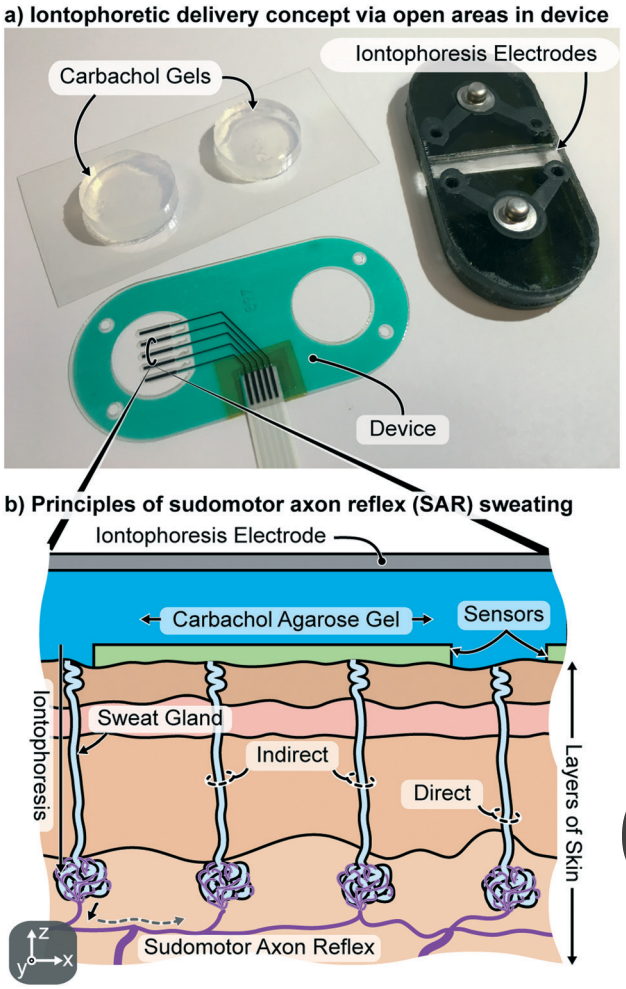

Fig. 1 Structure and function of SAR device. (a) Picture of the carbachol gels used for stimulation, the acrylic holder used for iontophoresis and the actual device, itself. (b) Illustration of a cross-section of the device on skin including the gels, device and sweat glands. (c) Illustration of the SAR device including dimensional specifications.

Bromophenol blue and silicone oil suspension

The 5000 cSt and 100 cSt cosmetic grade PDMS was mixed in a 1 : 3.5 ratio. To this solution, bromophenol blue was added to a concentration of 7% by weight. Bromophenol blue does not readily dissolve in PDMS and was further mixed with a vortex mixer and ultrasonic bath treatment to break apart large clumps before each use. These methods were based on the previous technique by Tashiro.[34]

Carbachol gelation process

The process for making carbachol gels included mixing the carbachol and agarose at concentrations of 1% and 3% by weight in deionized water, respectively. To aid in dissolution and the cross-linking process, this solution was heated on a hot plate set to 150 °C until the agarose had fully dissolved into solution. This dissolution period depended upon the amount of solution prepared, but was typically on the order of 15–20 minutes. After this period, the hotplate was reduced to 80 °C and the solution was given at least 15 minutes to equilibrate to this lowered temperature. Since water from accelerated evaporation is lost in the heating process, deionized water was added to the solution to bring the solution back to the original weight after the aforementioned equilibration period. The carbachol/agarose solution was then cast in an acrylic mold which provided an array of discs of 4 mm thickness and 17 mm diameter. The mold was placed into a refrigerator at ~8 °C where the discs were allowed to solidify. Finally, the carbachol discs were transferred from the mold after solidification to an air-tight container and stored at 5 °C until use.

ed From a Chip

Fabrication of the SAR device platform

Prior to printing of features, a PET substrate (324.67 cm^2) was thoroughly cleaned with isopropanol, dried and flattened between two aluminum sheets at 150 °C. After the PET substrate was allowed sufficient time to cool, carbon traces were printed using the flexible, screen printable carbon ink (CI-2001) followed by a curing step within a 100 °C oven for about 30 minutes. Similarly, silver/silver-chloride ink (CI-4001) was printed for the reference electrode and followed by a curing step within a 100 °C oven for about 30 minutes. Finally, a screen printable, flexible solder mask was printed for isolation and cured utilizing an ultraviolet light-curing conveyer primarily operating in the UV-A spectrum. Each of these printing steps were performed utilizing a manual squeegee process on a low-volume stencil printer (SP-5500, Manncorp, Huntingdon Valley, PA). The 12″ × 17″ patterned screen (Sefar, Inc., Depew, NY) used to print these features was broken up into three regions – one region for each of the three layers – to allow for printing of six devices on one 324.67 cm^2 PET substrate. After screen printing, the devices were identified with a 'Device ID' and cut into their ultimate shape *via* use of a 50 W CO_2 laser (Universal Laser Systems, VLS 3.50). Interface connectivity between the carbon traces and flexible flat cable (FFC) was made *via* *z*-axis conductive tape. To further increase adhesion, a piece of Kapton tape was added over this conductive stack and pressed onto the device with finger pressure. After completion, the device was cleaned

 This journal is © The Royal Society of Chemistry 2017

Published on 04 July 2017. Downloaded by UNIVERSITY OF CINCINNATI on 25/07/2017 20:27:51.

with deionized water and blown dry with nitrogen. Functionalization of the two sodium-sensitive electrodes on the screen-printed carbon traces utilized a process[11] developed by Eccrine Systems, Inc (Cincinnati, OH) utilizing a commonly available Na^+ ionophore (Sigma Aldrich, 71747) suspended in a PVC matrix. Additionally, the sodium sensors leveraged a PEDOT/PSS ion-to-electron transduction layer which was electrochemically deposited onto the carbon traces.[12] Each sensor was coated with 1.5 μL of ionophore solution (two 0.75 μL coats) which typically produced a sodium-sensitive membrane thickness on the order of 100 μm. The medical adhesive layer to interface between the device and skin was also cut to shape utilizing the previously described CO_2 laser system. The adhesive component was preserved until after calibration of the sensors to prevent wetting of the adhesive liner. The adhesive layer was applied to the device through the aid of alignment pins after calibration and before *in vivo* testing.

Calibration of sensors

All calibration was performed for each device shortly before and after on-skin testing through use of a stable, double-junction reference electrode (Sigma Aldrich, Z113107). Calibration of the two sodium sensors and Ag/AgCl reference was performed in three aqueous solutions in the following order: 20 mM NaCl & 2 mM KCl, 45 mM NaCl & 5 mM KCl and 100 mM NaCl & 15 mM KCl. Prior to each 'before test' calibration the device was allowed to equilibrate in 100 mM NaCl and 15 mM KCl (~1 h). During this conditioning period, the drift of the sensors was characterized after stabilization and each exhibited drift below 5 mV h^{-1}. Before introducing the device to a new solution, the device and calibration chamber were thoroughly cleaned with deionized water. By nature of the sensors themselves, the sodium-sensitive electrodes exhibited an increase in interfacial voltage for an increase in sodium concentration whereas the Ag/AgCl reference demonstrated a decrease in interfacial voltage for an increase in chloride concentration – each demonstrating a sub-Nernstian response.[24] As there were two, main interactive species in solution (Na^+, Cl^-), the cell potential exhibited a superficial super-Nernstian response on the order of 100 mV dec^{-1} depending on the specific device tested. For example, at a 'high' electrolyte concentration (100 mM NaCl, 15 mM KCl), the cell potential could exhibit a voltage of 140 mV. In this instance, this provides with 100 mM Na^+-interaction at the sodium-sensitive membrane and 115 mM Cl^--interaction at the chloride-sensitive electrode (Ag/AgCl reference). However, in a similar instance with a 'low' electrolyte concentration (20 mM NaCl, 2 mM KCl) the cell potential could exhibit a voltage of 70 mV. In the case of 'high' electrolyte concentration, the active ion species concentration is 215 mM (100 mM Na^+ + 115 mM Cl^-) and 'low' electrolyte concentration the active ion species totals 42 mM (20 mM Na^+ + 22 mM Cl^-). Therefore, fitting the logarithmic value of active ion concentrations to the observed voltages provides an estimate for the total sodium and chloride concentration. Since each contributes approximately half (ex., 100 mM Na^+ *vs.* 115 mM Cl^-) one can take the outputs of this fitted calibration curve and divide the resulting value in half for an estimate of both sodium and chloride concentrations – within reasonable accuracy. Selectivity of the sodium sensors to potassium was strong with the sodium sensor only exhibiting less than ±2 mV dec^{-1} response to potassium concentration changes for a given concentration range of 2–20 mM. After calibration, the sensors were rinsed, dried, then had the pre-cut medical adhesive placed on the device and taken to the subject for testing. After the test, the sensors were then calibrated again to ensure continuity in function of the device.

Data analysis

As there were two, main interactive species in solution (Na^+, Cl^-), the cell potential(s) exhibited a superficial super-Nernstian response on the order of 100 mV dec^{-1}. Since sweat sodium and chloride levels trend in the same direction in a relatively predictable manner with a 10–20 mM offset,[35] one can estimate both sodium and chloride levels as half of the concentration values that appear to be observed when the sodium sensors are in reference to a Ag/AgCl electrode. This is the approach taken here.

For the impedance data, a fixed 2.25 kHz, sinusoidal, 0.25 V amplitude waveform was utilized by the impedance spectroscopy module in the PSTrace 4.8 software to measure the skin impedance. Measurements were recorded every 30 s with a 2 s minimum sampling time and 5 s maximum equilibration time to help improve noise filtering and accuracy. Furthermore, the current compliance limit was fixed to a maximum of 100 μA to ensure subject safety even though the measurements typically required substantially less current.

On-skin testing

Human subjects testing was performed under the guidance of the University of Cincinnati's (UC) Human Research Protection Program. Further, the protocol presented here was reviewed and approved by the UC Institutional Review Board (IRB). Informed consent was obtained for all participants of this study (2015-5211).

First, the subject's arm was cleaned with isopropanol to remove sebum followed by deionized water to rehydrate the stratum corneum and finally dried with a paper towel to ensure no excess water remained on the skin. The device was then applied to the chosen location on the forearm. An acrylic mold encapsulating fresh carbachol gels and integrated stimulation electrodes, was aligned over the open areas in the device. This stimulation unit was secured with an elastic strap to ensure contact with the skin. This acrylic unit holding the stimulant gels remained on the skin for 2.5 minutes with no iontophoresis applied. After this time, the acrylic unit and gels were removed with the device remaining on the skin and data from the device recorded for a half hour ('No Iontoph. No Pressure'). After this time, the acrylic unit

Reprinted From
Lab on a Chip

Published on 04 July 2017. Downloaded by UNIVERSITY OF CINCINNATI on 25/07/2017 20:27:51.

Reprinted From Lab on a Chip

with gels were placed back on the skin for 2.5 minutes. As before, no iontophoresis was performed during this time. After the 2.5 minutes, the acrylic unit and gels were removed with the device remaining on the skin and a section of memory foam was placed over the sensor array with an elastic strap to help press the sensors towards the skin, thereby reducing the previously present dead volume. The pressure applied *via* this memory foam pad was estimated at 0.8 kPa with use of a force-sensitive resistor (FSR). Data was then collected for a half hour ('No Iontoph. + Pressure'). Finally, the acrylic unit with fresh gels was placed onto the skin. Iontophoresis was performed for 2.5 minutes at a current of 0.2 mA (approximately 0.25 mA cm^{-2}) resulting in a dosage metric of 30 mC. This dosage metric is merely an estimation of an unquantifiable amount of sweat stimulant (carbachol) that is introduced through the skin. Impurities from the skin, agarose and water do not result in a 1 : 1 relationship between current (charge) flow and actual drug delivered.[36] After the stimulation period, the acrylic unit and gels were removed whilst the device again remained on the skin. Similar to the technique previously, a section of memory foam with an elastic strap was placed on the skin to reduce the gap between sensor and skin. Data from the device was recorded for a half hour ('Iontoph. + Pressure'), after which the device was removed and testing completed.

For the case of one subject (subject D, Fig. 5), a shortened & alternative procedure was performed where iontophoresis was applied over the open areas of the device utilizing the setup and settings described above. However, instead of data collection from the sensors, the device was subsequently removed and the dye solution was placed on the skin for imaging of activation of sweat glands. The solution was placed on the skin 3 minutes after stimulation and then images were taken 5 minutes after the placement of the dye (8 total minutes after iontophoresis).

Results and discussion

Choice of sweat stimulant

A significant concern for devices which employ a pharmacological agent for sweat stimulation is the required dosage to stimulate sufficient sweat production. For some sweat stimulants that produce a SAR response, such as acetylcholine, their metabolic lifetime is rather short for they are quickly metabolized by acetylcholinesterase (AChE, see Table 1), an enzyme present around the sweat gland.[37] For this reason, alternative options to commonly selected stimulants must be chosen[1] (Table 1). The device described within makes no exception to this clause and utilizes a sweat stimulant used for a variety of cholinergic interactions called carbamylcholine or carbachol (CCh). Carbachol has been previously shown to provide a SAR response[38–41] and is also poorly metabolized by acetylcholinesterase.[42–44] Therefore, carbachol causes prolonged neuroglandular interactions – effectively reducing the amount of drug required to sustain a response (see discussion section).

Device design

Shown in Fig. 1a and c is the complete device structure – to scale – with specific details of fabrication described in the Experimental section. The device has two open areas for gel contact, one being the iontophoretic area where carbachol is delivered through the skin and the return electrode area which provides a return path for the current source. The sensing array includes 5 total electrodes in a symmetric manner: impedance electrode|Na^+ sensor|Ag/AgCl reference|Na^+ sensor|impedance electrode. This provides two unique sensing mechanisms with two sodium sensors in reference to a Ag/AgCl electrode and one impedance measurement requiring the pair of impedance electrodes for sampling. Electrode interfacing is achieved *via* *z*-axis conductive tape to transverse from the carbon traces to a FPC cable which is connected externally to the measurement equipment (see Experimental section).

To further maximize the effectiveness of a SAR response, this device utilizes 'finger-like' sensors with high y/x aspect ratio as shown in the 'zoomed sensor view' of Fig. 1c. Since SAR requires axonal conduction towards branch points which then produce secondary signals, it is beneficial to minimize lateral distances between the edge of iontophoresis and center of the sensor. For example, the rectangular sensors of this device shown in Fig. 1c have an area of 2.5 mm^2 with a distance of 0.75 mm from edge-to-center (includes extended PET substrate for adhesive boundary, discussed later). For a circular sensor of comparable area, the center to edge distance would be 1.39 mm or 85% longer distance (also includes native 0.5 mm edge offset for adhesive). As a sensor's edge-to-center distance decreases (Fig. 1c), the distance required for an axon-reflex-mediated signal to activate glands underneath the sensor also decreases and therefore less stimulant dosage is needed.

To provide added perspective to the reader, Fig. 2 shows a cross-sectional, pictorial view of slightly more than half of the device on skin (three electrodes exposed). As shown in Fig. 2 and alluded in Fig. 1c, each electrode was surrounded with an adhesive boundary to isolate the sensing regions and stimulation area. The thickness of this medical adhesive per the specifications of the manufacturer is 3.6 mil (~92 μm). As shown in the diagram, the process of coating the Na^+ ion-selective membranes provided some overlap into the PET-substrate area designated for adhesive. To help alleviate the possibility of adhesive delamination during testing and promote sweat to sensor contact, even pressure was applied across the device during a portion of data collection (see Experimental section).

Characterization of adhesive isolation

One concern for a device with separated stimulation and sensing regions is keeping each section isolated from the other. Fig. 3 shows the isolation capabilities and limitations of the medical adhesive used. This was performed by laser machining the testing pattern with line/space/line features of

 This journal is © The Royal Society of Chemistry 2017

Published on 04 July 2017. Downloaded by UNIVERSITY OF CINCINNATI on 25/07/2017 20:27:51.

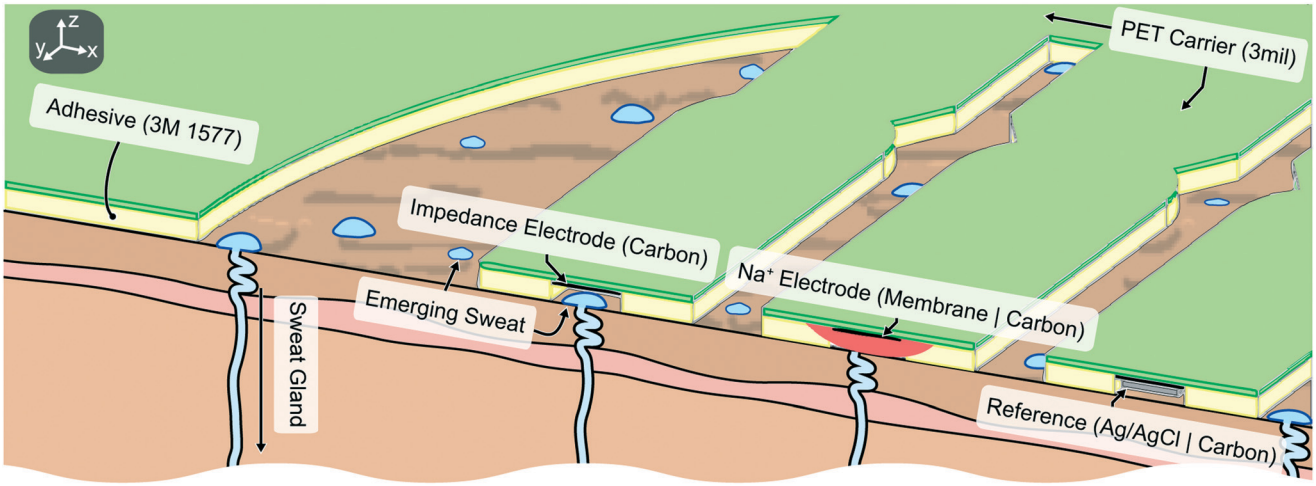

Fig. 2 Cross-sectional illustration of the SAR device on skin where further details on device operation and materials utilized are presented.

0.1 mm, 0.2 mm, 0.3 mm, 0.4 mm, 0.5 mm, 0.8 mm and 1 mm (left to right, Fig. 3). This testing pattern was placed on the skin and a blue-dye-saturated cotton swab was pressed on the skin to simulate a hydrogel. After several minutes the swab was removed and the ability of the adhesive to block transversal movement of the dye was observed. The minimum acceptable adhesive width was determined at 0.5 mm, with smaller features providing questionable or poor isolation (observed as the lack of a gap between blue lines in Fig. 3). It should be noted that the 0.5 mm feature is not the actual width of the final cut adhesive. Rather, due to the spot size of the cutting laser the actual adhesive width is slightly smaller – an estimated 425 to 475 μm. Regardless, the nominal 0.5 mm adhesive width was determined to be ideal for isolation between the sweat stimulation (open area) and sensors themselves. Larger adhesive widths could be used, but they would increase the distance between directly and indirectly stimulated regions, which would then require higher doses of stimulant.

In vitro calibration of sensors

Calibration of the sodium sensors utilized a three-point calibration system of varying concentrations within expected ranges for sweat (see Experimental section). Condensed calibration data of one device's sodium sensors before and after on-skin testing is demonstrated in Fig. 4. The roughly +70 mV response before and after on-skin testing correlates to a 98 mV dec^{-1} response as a result of the sub-Nernstian contributions at the sodium and reference electrodes with Na^+ and Cl^-, respectively.[11,26,45,46] The origin of the apparent super-Nernstian response is a result of interactions which occurs at both the sensing (sodium) and reference electrodes (chloride). Please refer to the Experimental section for more details on the assumptions of this analysis technique. While this test itself is simple in nature, it provides valuable insight to not only the functionality of the sensors before and after testing but also any deviations from expected data.

In vivo results

To ensure sweat production underneath the sensor array and further validate the SAR approach, direct observation of sweat

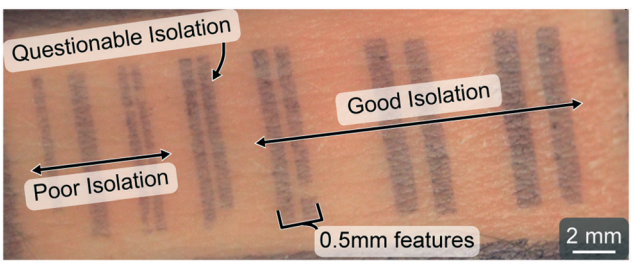

Fig. 3 Simple test for isolation capabilities of medical adhesive on skin utilizing a blue dye.

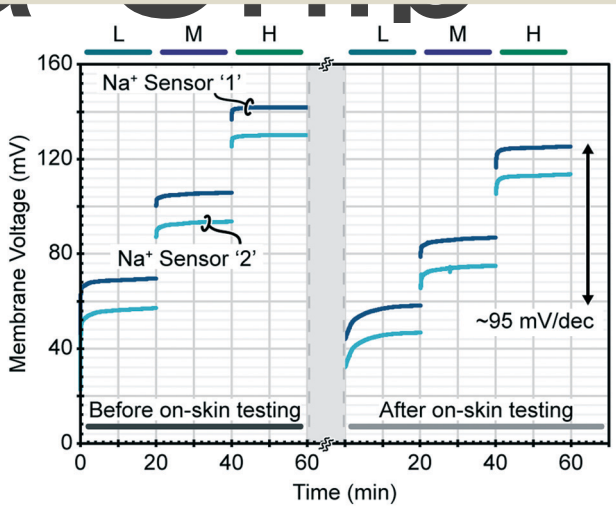

Fig. 4 Example of calibration data for two Na^+ sensors (in reference to the Ag/AgCl electrode) on one device before (left) and after (right) on-skin testing. Each sensor varied slightly in response, however, most exhibited roughly 98 mV dec^{-1} change in Na^+/Cl^- concentration. The key at the top of the plot shows three calibration solutions: L – low, 20 mM NaCl and 2 mM KCl; M – medium, 45 mM NaCl and 5 mM KCl; H – high, 100 mM NaCl 15 mM KCl.

Reprinted From Lab on a Chip

Published on 04 July 2017. Downloaded by UNIVERSITY OF CINCINNATI on 25/07/2017 20:27:51.

gland activation was performed. This process involved the same sweat stimulation procedure as will be described shortly, however, instead of recording data from the sensor array the device was removed completely and a pH-sensitive dye (bromophenol blue) was used to monitor sweat production. In this technique, bromophenol blue is suspended in a cosmetic grade silicone oil[47] so that sweat produced at the oil interface causes extraction of bromophenol blue molecules which interact with the slightly acidic nature of sweat[35] causing an orange to blue color change. Fig. 5 shows the results of this test with Fig. 5c showing a zoomed, overlay of the images presented in Fig. 5a and b. The image of Fig. 5b was taken roughly 8 minutes after completion of iontophoresis (pH sensitive dye on skin for 5 minutes) and shows a relatively even distribution of sweat gland activation with no obvious exclusion underneath the 'finger-like' sensors of the device. Assuming a gland density of 100–150 glands per cm^2 present on the forearm[48] and sensor area of 2.5 mm^2 this presents with an approximate 3+ glands which should be activated underneath the footprint of the sensor (carbon trace) assuming a strong SAR response. The results of Fig. 5c corroborate this assumption within reasonable expectation and provide further confidence in the efficacy of SAR sweating for sweat biomarker sensing.

Complete device demonstrations including sensor readings for three subjects are presented in Fig. 6, showing four different metrics: capacitance, resistance, reactance and sodium sensor data. Additionally, there are three different scenarios presented as illustrated on the top of Fig. 6 for each subject: an instance of no iontophoresis and no sensor compression ('No Iontoph. No Pressure'), no iontophoresis with sensor compression ('No Iontoph. + Pressure') and iontophoresis with sensor compression ('Iontoph. + Pressure'). Briefly, each one of these scenarios describes whether sweat was elicited *via* iontophoresis prior to data collection and if during measurements the sensor array was compressed with memory foam to reduce the gap between the sensor and skin. In Fig. 6 the blue columns represent the time at which gels were placed over the device and iontophoresis was performed ('Iontoph.') or not performed ('No Iontoph.'). The equivalent capacitance data of Fig. 6 illustrates the effects of reducing the sensor dead volume (gap) and effects of sweating. This

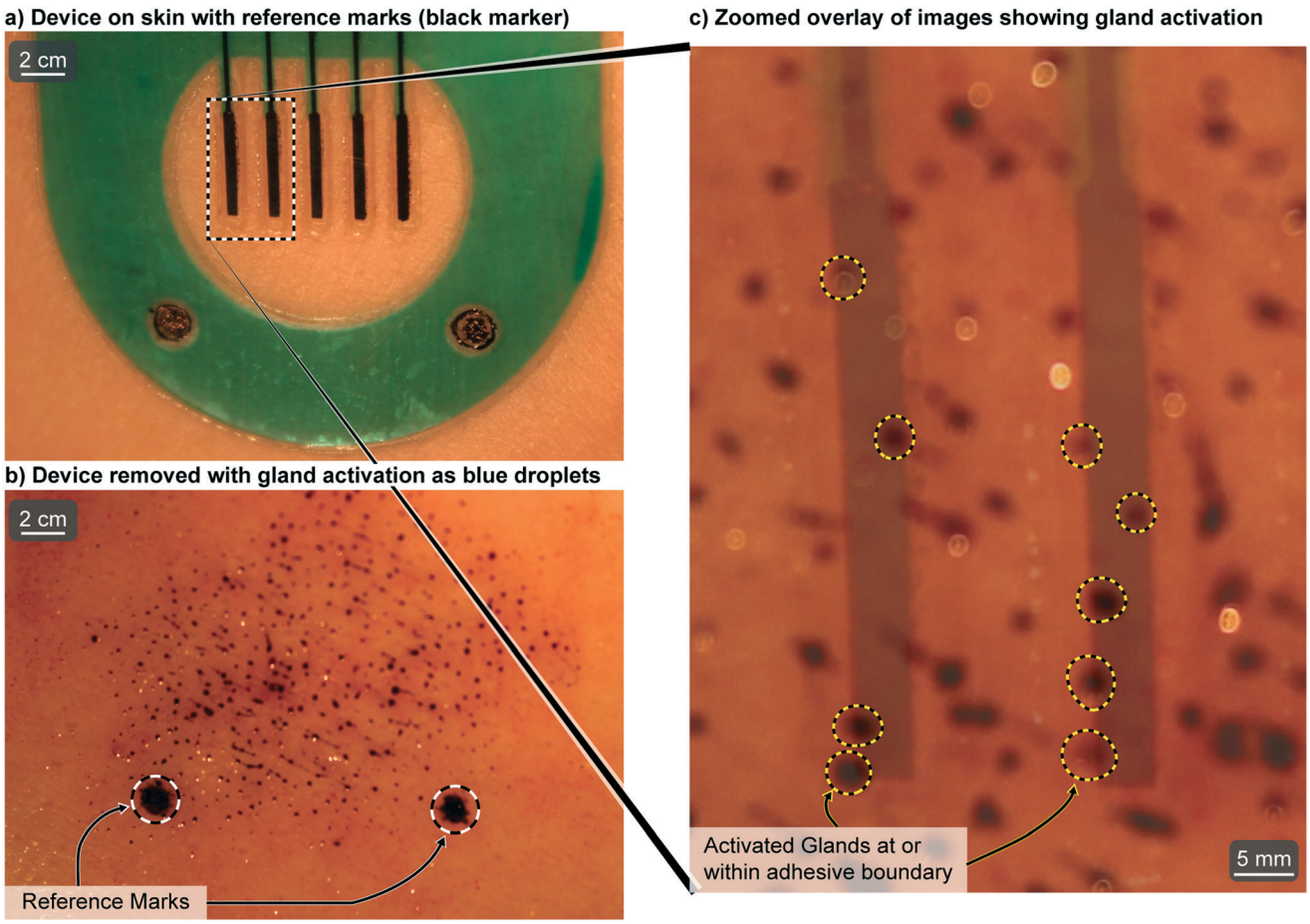

Fig. 5 Images of skin showing the activation of sweat glands from carbachol iontophoresis. (a) Before iontophoresis, an image of the skin with the device was recorded including a couple of marks with permanent marker for alignment of post-iontophoresis photos in (c). (b) Image of the skin after iontophoresis with a pH-sensitive dye to highlight gland activation. Image was taken 8 minutes after iontophoresis and 5 minutes after application of the dye solution. Towards the top-right of the image there is apparent SAR-induced sweat production. (c) Overlaid image of (a) and (b) to assess activation of glands underneath sensors.

 This journal is © The Royal Society of Chemistry 2017

Published on 04 July 2017. Downloaded by UNIVERSITY OF CINCINNATI on 25/07/2017 20:27:51.

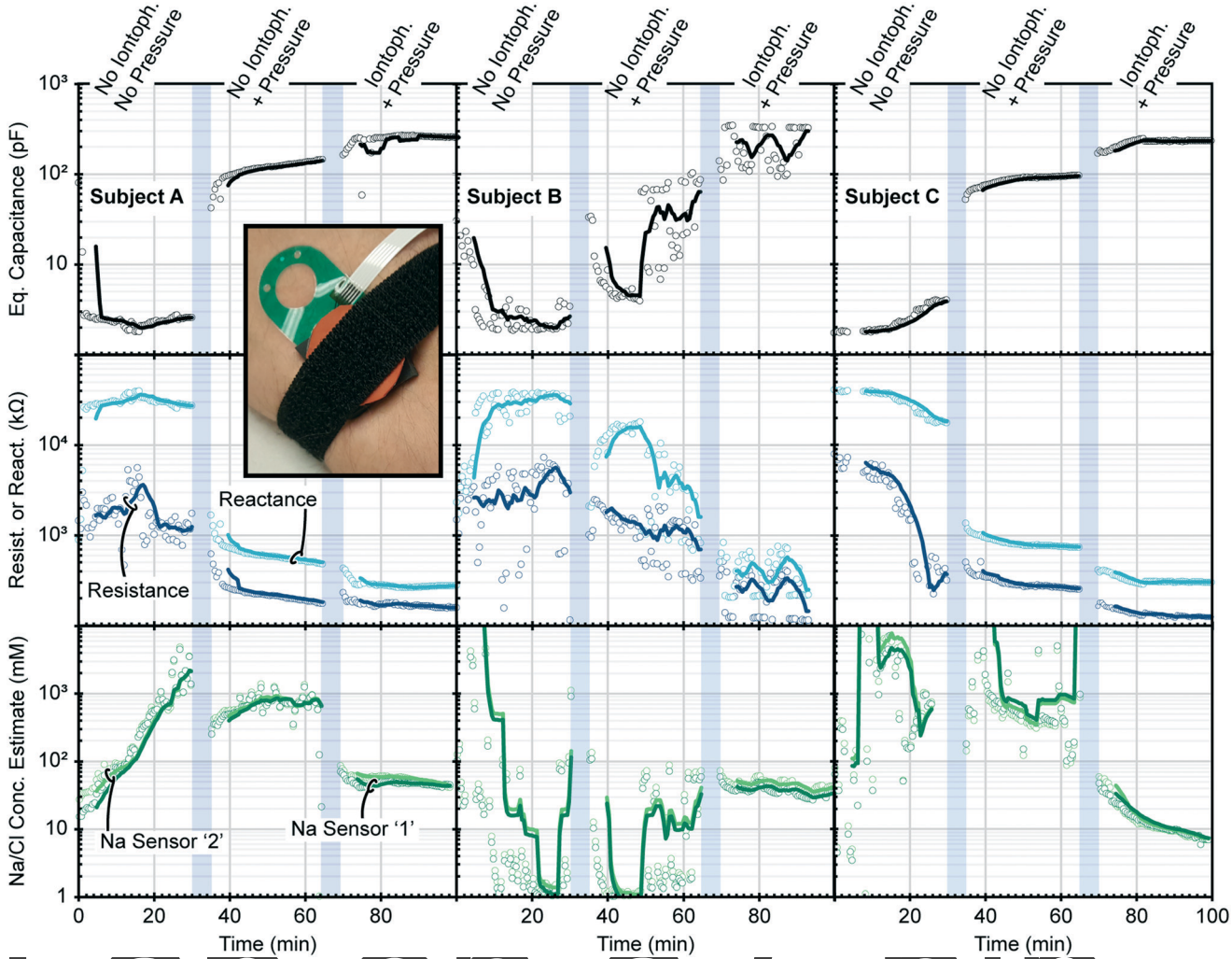

Lab on a Chip

Fig. 6 Capacitance, resistance or reactance and Na^+/Cl^- concentration estimate plots for three subjects (subject A, B & C). As part of the procedure, each subject had three sections of measurement including an instance of no iontophoresis and no pressure applied, no iontophoresis with pressure applied, and iontophoresis with pressure applied, respectively. The blue columns separating each region are times when the carbachol gels were placed onto the skin and iontophoresis (or no iontophoresis in the first two cases) was performed – see the Experimental section for details. Inset photo shows a device on a subject's skin with compressive memory foam and strap. For the plots shown here, the solid lines represent a 10-point (5 minute) moving average. Further, the points shown for Na^+/Cl^- estimates are a result of a 30 s-median filter applied to the original data (native sample interval ~0.167 s).

capacitance value is a calculated value from the sensing equipment *via* the reactance values from the impedance electrodes and analyzed assuming an equivalent resistive and capacitive network. In accordance with the following equation, $C = \varepsilon_0\varepsilon_r[A/d]$, as the distance d between conductive elements decreases, the capacitance C increases.[49] Furthermore, as the relative permittivity ε_r increases (*e.g.* sweat *vs.* air), the observed capacitance will increase. The sensor area A and vacuum permittivity constant ε_0 are assumed to remain unchanged in this instance. The results of Fig. 6 demonstrate this concept with a significant increase in capacitance with application of pressure to the sensor array onto the skin (reducing d). Additionally, once sweating occurs ('Ionto. + Pressure') the capacitance increases further because sweat, which is mostly water,[8] has a substantially higher relative permittivity compared to air.[50] Due to the complex nature of skin and inevitable variability between subjects, predictive modeling is difficult, although compelling demonstrations have been previously presented.[51] In the case of sweat event sensing, however, utilization of a simple and qualitative metric for detecting sweat events such as capacitive sensing could prove useful for future technologies.

To a first order, skin impedance can be utilized as a further improvement to capacitive analytical techniques to address quantification of sweat rate.[8] Sweat rate is an important biomarker not necessarily for the health or athletic information it provides, but more importantly because many analytes in sweat are strongly dependent upon sweat rate.[8] The first region of Fig. 6 for each subject ('No Iontoph. No Pressure') show erratic measurements from the impedance sensors at magnitudes generally above 1 MΩ, indicative of a no or low-sweat-rate instance. These artifacts are expected due to

Published on 04 July 2017. Downloaded by UNIVERSITY OF CINCINNATI on 25/07/2017 20:27:51.

Reprinted From Lab on a Chip

instability of skin contact and/or lack of sweat contact to complete the measurement circuit. This situation is improved in the second region ('No Iontoph. + Pressure') as contact between the sensors and skin is improved with compression. However, once sweating is initiated and the sensor-skin gap minimized ('Iontoph. + Pressure') the resistance and reactance measured at the skin surface is observed with lower magnitude and variation (noise). While the extended time dependence of carbachol-induced SAR sweating is not demonstrated in this figure (only a half hour of data collected for brevity), the authors note that sweating *via* carbachol was reported to persist in diminished capability in at least the directly stimulated regions for extended periods of time (5+ hours) due to the limited ability of acetylcholinesterase to metabolize carbachol.[1] It is likely that sweat production in indirect (axon reflex) regions is shorter lived than the direct response per limited, previous literature which has demonstrated SAR sweating from carbachol on the order of 1–2 hours.[41] This conclusion requires more investigation outside the scope of this manuscript as smaller devices such as that presented here could extend indirect stimulation time due to lateral iontophoretic or diffusional effects as discussed previously (speculative). Additionally, the duration of sweating is potentially extendable by repeating the stimulation as needed – this too requires further investigation outside the scope of this work.

The sodium and chloride estimated concentrations in Fig. 6 provide a secondary and perhaps complementary method to quantify sweat rate in detail. Noise in the first two regions ('No Iontoph. No Pressure' & 'No Ionto. + Pressure') is a symptom of poor electrode contact to skin/sweat as observed in the impedance electrodes. The cell potential begins to steady and converge in the third region where sweat is produced underneath the sensors. These values on the order of 10–50 mM Na^+/Cl^- are on par with expected concentration values for sweat. This concentration range assumes that the measured cell potential voltages are a result of the shared contributions of Na^+ and Cl^- at the sodium-sensitive membrane(s) and reference electrode, respectively. In actuality, the Na^+ concentration is higher than Cl^- potentially up to 20 mM which could mask the accuracy of this technique.[35] Regardless, the simplicity of this approach does not require an encapsulated reference which presents significant technological hurdles for sensors at this scale. Utilizing a bare Ag/AgCl reference as presented here improves response time, flexibility, leakage and manufacturability typically exhibited from encapsulated configurations – for a small sacrifice in data accuracy. It is also hypothesized that further improvements to this technique could be improved from the measurement of other ions present within sweat. Carbonate (HCO_3^-), the other predominate anion in sweat, bridges the vast majority of the 10–20 mM gap between sodium and chloride for charge neutrality[35] and a carbonate-sensitive sensor could further improve accuracy of chloride estimations thereby improving sodium estimations as well. Furthermore, inclusion of a relatively sweat-rate-independent electrolyte, such as potassium, could provide a strong reference to stabilize sweat rate estimations that are based on a combination of electrolyte and skin impedance observations.[35] As mentioned previously, an ability to quantify sweat rate in a more reliable manner[51] would improve the diagnostic capabilities of sodium and chloride concentrations. The authors direct the reader towards the Experimental section for further details. Additionally, since the electrical path from the sodium-sensitive membrane(s) to reference electrode requires through-skin electrical propagation (because of the adhesive isolation), this potentially introduces additional impedance and voltage fluctuations[52] to the 'circuit'. This could skew the observed voltages of a voltmeter from the actual voltage present between the sodium-sensitive membrane(s) and reference electrode. For the test described in this manuscript, however, an optically isolated data acquisition system with high input impedance (10^{13} Ω) was utilized ensuring that the impedance of the measurement unit was many orders of magnitude greater than the impedance of the measuring 'circuit' (sensors & skin). In an ideal situation, sweat could be wicked from the indirect stimulation regions to an isolated sensor array whereby a lower-impedance path between sensor and reference electrodes is obtained.

Drift appears to be present during the third region ('Iontoph. + Pressure'). The exact cause of this drift on the skin and during calibration (~5 mV h^{-1}) is unknown and could be due to one or multiple causes. Such causes could include sample leakage through the membrane, secondary membrane interactions such as non-idealities at the membrane/ion-transduction layer, unintended interactions at the reference electrode, and/or the very high-impedance of the sensor. One additional source of drift could be due to the pressure used to hold the device and sensors onto the skin. The sodium-sensitive membrane has a thickness substantially thicker than the impedance electrodes (screen-printed carbon) or reference electrode (screen-printed Ag/AgCl on screen-printed carbon). Thus, the sodium-sensitive membranes have a thickness on par with the thickness of the adhesive providing a diminutive gap between sensor and skin. The pressure applied further decreases this gap and introduces a potentially unknown relationship between sensor response and applied pressure.[53] We speculate that future designs with this SAR device will likely replace the sensors with a wicking material that transports sweat to sensors away from skin. Also worth mentioning for the sensor results on skin, the skin presents an electrically and chemically noisy surface which could skew the sensor signal and/or the concentrations of analytes in sweat.[47,52]

Conclusions

The sweat stimulation and sensing device presented within this manuscript provides a compelling technique with potential to enable continuous sweat biomarker sensing – even for resting individuals. Most importantly, this work opens the door to the ability for side-by-side integration of chemical

 This journal is © The Royal Society of Chemistry 2017

Published on 04 July 2017. Downloaded by UNIVERSITY OF CINCINNATI on 25/07/2017 20:27:51.

stimulants & sensors without cross-contamination and integration compatible with both enzymatic sensors & sensors which equilibrate with analyte concentrations. Furthermore, the sensors demonstrated here are those which are likely to accompany other electrochemical sensor(s), because the demonstrated sensors can potentially be used to predict sweat generation rate and therefore the sampling rate for a device.

An additional and important point of discussion is the possibility for a combination of direct and an indirect SAR response underneath the sensors. The dermis is typically several millimeters thick and filled with porous collagen[30] and interstitial fluid. The receptor sites for stimulation are at the base of the sweat glands,[29,30] and the sensor fingers are so narrow that partial horizontal diffusion and/or partial horizontal iontophoretic delivery of carbachol may be possible on a small enough scale. However, such determination of which mechanism dominates is immaterial, as the smart integration scheme presented here works as needed in either situation.

Finally, the management of sweat generation, which can be simply wicked away from the sensors and stimulation regions using wicking materials is a topic of future work for our research group. While this device does not provide an exhaustive assessment of biomarkers present within sweat as can be found elsewhere,[7,15,35] this device demonstrates the plausibility of an effective and convenient sweat stimulation and analysis device for individuals at rest.

Reprinted From
Lab on a Chip

Competing financial interests

The corresponding author (Heikenfeld) also discloses a potential conflict of interest as he is a co-founder of Eccrine Systems Inc. which is commercializing sweat sensing technologies.

Acknowledgements

The authors acknowledge support from the National Science Foundation and the industrial members of the Center for Advanced Design and Manufacturing of Integrated Microfluidics (NSF I/UCRC award number IIP-1362048), the Air Force Research Labs Award #USAF contract # FA8650-15-C-6625, and from NSF EPDT Award #1608275.

References

1 H. P. Rang, M. M. Dale, J. M. Ritter and R. J. Flower, *Rang and Dale's Pharmacology*, Churchill Livingstone, Edinburgh, Philadelphia, 6th edn, 2007.
2 S. Patel, H. Park, P. Bonato, L. Chan and M. Rodgers, *J. Neuroeng. Rehabil.*, 2012, **9**, 1–17.
3 A. J. Bandodkar and J. Wang, *Trends Biotechnol.*, 2014, **32**, 363–371.
4 M. X. Chu, K. Miyajima, D. Takahashi, T. Arakawa, K. Sano, S.-I. Sawada, H. Kudo, Y. Iwasaki, K. Akiyoshi and M. Mochizuki, *Talanta*, 2011, **83**, 960–965.
5 J. Heikenfeld, *Nature*, 2016, **529**, 475–476.
6 N. De Giovanni and N. Fucci, *Curr. Med. Chem.*, 2013, **20**, 545–561.
7 A. Mena-Bravo and M. D. Luque de Castro, *J. Pharm. Biomed. Anal.*, 2014, **90**, 139–147.
8 Z. Sonner, E. Wilder, J. Heikenfeld, G. Kasting, F. Beyette, D. Swaile, F. Sherman, J. Joyce, J. Hagen and N. Kelley-Loughnane, *Biomicrofluidics*, 2015, **9**, 031301.
9 M. Calderón-Santiago, F. Priego-Capote, N. Turck, X. Robin, B. Jurado-Gámez, J. C. Sanchez and M. D. L. De Castro, *Anal. Bioanal. Chem.*, 2015, **407**, 5381–5392.
10 M. Calderón-Santiago, F. Priego-Capote, B. Jurado-Gámez and M. D. Luque de Castro, *J. Chromatogr. A*, 2014, **1333**, 70–78.
11 D. P. Rose, M. Ratterman, D. K. Griffin, L. Hou, N. Kelley-Loughnane, R. R. Naik, J. A. Hagen, I. Papautsky and J. Heikenfeld, *IEEE Trans. Biomed. Eng.*, 2014, **62**, 1457–1465.
12 W. Gao, S. Emaminejad, H. Y. Y. Nyein, S. Challa, K. Chen, A. Peck, H. M. Fahad, H. Ota, H. Shiraki, D. Kiriya, D.-H. Lien, G. A. Brooks, R. W. Davis and A. Javey, *Nature*, 2016, **529**, 509–514.
13 J. Kim, W. R. de Araujo, I. A. Samek, A. J. Bandodkar, W. Jia, B. Brunetti, T. R. L. C. Paixão and J. Wang, *Electrochem. Commun.*, 2015, **51**, 41–45.
14 A. J. Bandodkar, D. Molinnus, O. Mirza, T. Guinovart, J. R. Windmiller, G. Valdés-Ramírez, F. J. Andrade, M. J. Schöning and J. Wang, *Biosens. Bioelectron.*, 2014, **54**, 603–609.
15 S. O. García, Y. V. Ulyanova, R. Figueroa-Teran, K. H. Bhatt, S. Singhal and P. Atanassov, *ECS J. Solid State Sci. Technol.*, 2016, **5**, M3075–M3081.
16 A. Koh, D. Kang, Y. Xue, S. Lee, R. M. Pielak, J. Kim, T. Hwang, S. Min, A. Banks and P. Bastien, *Sci. Transl. Med.*, 2016, **8**, 366ra165.
17 X. Huang, Y. Liu, K. Chen, W. J. Shin, C. J. Lu, G. W. Kong, D. Patnaik, S. H. Lee, J. F. Cortes and J. A. Rogers, *Small*, 2014, **10**, 3083–3090.
18 J. B. Sloan and K. Soltani, *J. Am. Acad. Dermatol.*, 1986, **15**, 671–684.
19 A. K. Banga and Y. W. Chien, *J. Controlled Release*, 1988, **7**, 1–24.
20 M. Meloun and P. Černohorský, *Talanta*, 2000, **52**, 931–945.
21 H. C. Losty, H. Wheatley and I. Doull, *Ann. Clin. Biochem.*, 2006, **43**, 375–381.
22 J. Heikenfeld, *Electroanalysis*, 2016, **28**, 1242–1249.
23 J. Kim, I. Jeerapan, S. Imani, T. N. Cho, A. Bandodkar, S. Cinti, P. P. Mercier and J. Wang, *ACS Sens.*, 2016, **1**, 1011–1019.
24 F.-G. Bănică, *Chemical Sensors and Biosensors Fundamentals and Applications*, John Wiley and Sons, Inc., West Sussex, UK, 2012.
25 D. D. Cunningham, *Transdermal Microfluidic Continuous Monitoring Systems*, 2009.
26 S. Emaminejad, W. Gao, E. Wu, Z. A. Davies, H. Y. Y. Nyein, S. Challa, S. P. Ryan, H. M. Fahad, K. Chen and Z. Shahpar, *Proc. Natl. Acad. Sci. U. S. A.*, 2017, 201701740.
27 P. A. Low, T. L. Opfer-Gehrking and M. Kihara, *Clin. Auton. Res.*, 1992, **2**, 29–34.

Published on 04 July 2017. Downloaded by UNIVERSITY OF CINCINNATI on 25/07/2017 20:27:51.

28 P. A. Low, *Clin. Neurophysiol.*, 2004, **115**, 1506–1513.
29 M. J. Hilz, F. B. Axelrod, A. Bickel, B. Stemper, M. Brys, G. Wendelschafer-Crabb and W. R. Kennedy, *Brain*, 2004, **127**, 2090–2098.
30 W. Montagna, A. M. Kligman and K. S. Carlisle, *Atlas of Normal Human Skin*, Springer-Verlag New York, Inc., Malaysia, 1992.
31 B. Riedl, M. Nischik, F. Birklein, B. Neundörfer and H. O. Handwerker, *J. Auton. Nerv. Syst.*, 1998, **69**, 83–88.
32 M. Kihara, T. L. Opfer-Gehrking and P. A. Low, *Muscle Nerve*, 1993, **16**, 655–660.
33 P. A. Low, P. E. Caskey, R. R. Tuck, R. D. Fealey and P. J. Dyck, *Ann. Neurol.*, 1983, **14**, 573–580.
34 G. Tashiro, M. Wada and M. Sakurai, *J. Invest. Dermatol.*, 1961, **36**, 3–4.
35 K. Sato, W. H. Kang, K. Saga and K. T. Sato, *J. Am. Acad. Dermatol.*, 1989, **20**, 537–563.
36 D. Marro, Y. N. Kalia, M. B. Delgado-Charro and R. H. Guy, *Pharm. Res.*, 2001, **18**, 1709–1713.
37 M. Shibasaki and C. G. Crandall, *J. Appl. Physiol.*, 2001, **90**, 757–762.
38 B. Riedl, T. Beckmann, B. Neundörfer, H. O. Handwerker and F. Birklein, *Acta Neurol. Scand.*, 2001, **103**, 27–34.
39 C. Braune, F. Erbguth and F. Birklein, *Br. J. Dermatol.*, 2001, **144**, 111–117.
40 F. Birklein, R. Sittl, A. Spitzer, D. Claus, B. Neundörfer and H. Handwerker, *Pain*, 1997, **69**, 49–54.
41 E. Lang, A. Spitzer, D. Claus, B. Neundörfer and H. O. Handwerker, *Acta Neurol. Scand.*, 1995, **91**, 251–254.
42 J. Longmore, B. Jani, C. Bradshaw and E. Szabadi, *Br. J. Clin. Pharmacol.*, 1986, **21**, 131–135.
43 A. Hai, D. Ben-Haim, N. Korbakov, A. Cohen, J. Shappir, R. Oren, M. E. Spira and S. Yitzchaik, *Biosens. Bioelectron.*, 2006, **22**, 605–612.
44 D. Fayuk and J. L. Yakel, *Mol. Pharmacol.*, 2004, **66**, 658–666.
45 E. Bakker and M. E. Meyerhoff, *Anal. Chim. Acta*, 2000, **416**, 121–137.
46 R. D. Johnson and L. G. Bachas, *Anal. Bioanal. Chem.*, 2003, **376**, 328–341.
47 R. Peng, Z. Sonner, A. Hauke, E. Wilder, J. Kasting, T. Gaillard, D. Swaille, F. Sherman, X. Mao, J. Hagen, R. Murdock and J. Heikenfeld, *Lab Chip*, 2016, **16**, 4415–4423.
48 N. A. Taylor and C. A. Machado-Moreira, *Extrem Physiol Med*, 2013, **2**, 1–29.
49 I. M. Filanovsky, in *The Electronics Handbook*, ed. J. C. Whitaker, Taylor and Francis, Boca Raton, FL, 2nd edn, 2005, pp. 176–178.
50 M. Uematsu and E. U. Franck, *J. Phys. Chem. Ref. Data*, 1980, **9**, 1291–1306.
51 C. Tronstad, H. Kalvøy, S. Grimnes and Ø. G. Martinsen, *Ann. Biomed. Eng.*, 2013, **41**, 1074–1083.
52 S. Grimnes, A. Jabbari, Ø. G. Martinsen and C. Tronstad, *Skin Res. Technol.*, 2011, **17**, 26–34.
53 B. Müller and P. C. Hauser, *Anal. Chim. Acta*, 1996, **320**, 69–73.
54 T. Guinovart, A. J. Bandodkar, J. R. Windmiller, F. J. Andrade and J. Wang, *Analyst*, 2013, **138**, 7031–7038.
55 K. Mitsubayashi, M. Suzuki, E. Tamiya and I. Karube, *Anal. Chim. Acta*, 1994, **289**, 27–34.
56 L. S. Selva Kumar, X. Wang, J. Hagen, R. Naik, I. Papautsky and J. Heikenfeld, *Anal. Methods*, 2016, **8**, 3440–3444.

Reprinted From
Lab on a Chip

 This journal is © The Royal Society of Chemistry 2017